

## Research article

Dmitry N. Gulkin, Anna A. Popkova, Boris I. Afinogenov, Daniil A. Shilkin, Kęstutis Kuršelis, Boris N. Chichkov, Vladimir O. Bessonov and Andrey A. Fedyanin\*

# Mie-driven directional nanocoupler for Bloch surface wave photonic platform

<https://doi.org/10.1515/nanoph-2021-0295>

Received June 12, 2021; accepted August 1, 2021;

published online August 16, 2021

**Abstract:** Modern integrated photonic platforms should combine low-loss guiding, spectral flexibility, high light confinement, and close packing of optical components. One of the prominent platforms represents a one-dimensional photonic crystal combined with dielectric nanostructures that manipulate low-loss Bloch surface waves (BSWs). Proper design of nanostructures gives rise to a variety of optical resonances suitable for efficient capturing and controlling light. In this work, we achieve color-selective directional excitation of BSWs mediated by Mie resonances in a semiconductor nanoparticle. We show that a single silicon nanoparticle can be used as a subwavelength multiplexer switching the BSW excitation direction from forward to backward within the 30 nm spectral range with its central wavelength governed by the nanoparticle size. Our work opens a route for the on-demand fabrication

of photonic nanocouplers with tailored optical properties and submicron footprint.

**Keywords:** Bloch surface waves; laser-induced backward transfer; leakage radiation microscopy; Mie resonances; multiplexer; silicon nanoparticles.

## 1 Introduction

Controlling light in two-dimensional integrated circuits is one of the most prominent challenges of modern nanophotonics. It is particularly relevant for the development of quantum communications [1], optomechanical manipulation [2], and lab-on-a-chip technologies [3]. To date, silicon-based structures have received the most attention as a platform for two-dimensional optics, providing an excellent performance in the infrared spectrum and being compatible with conventional microfabrication techniques [4]. The use of surface electromagnetic waves, primarily surface plasmon–polaritons, presents a promising alternative to silicon photonics and allows one to significantly reduce the mode size and the dimensions of integrated photonic devices [5].

One-dimensional photonic crystals present a unique class of multilayer structures characterized by a diversity of propagating and localized optical modes [6–9]. In particular, Bloch surface waves (BSWs) supported by photonic crystals [10, 11] have been recently proposed as a novel platform for two-dimensional integrated photonics [12, 13]. In contrast to plasmonic structures, photonic crystals are typically made of dielectric materials and exhibit lower optical loss, which enables reaching a BSW propagation length of up to several millimeters [14]. The proper design of photonic crystals allows one to actually get rid of radiation losses, reducing them to a level of 1 dB/km in BSW waveguides [15]. Moreover, dispersion curves of BSWs can be varied by altering the photonic crystal parameters that makes them especially attractive for applications in the visible range [16, 17]. Currently, the main elements of BSW-based integrated optics including

Dmitry N. Gulkin and Anna A. Popkova contributed equally to this work.

\*Corresponding author: Andrey A. Fedyanin, Faculty of Physics, Lomonosov Moscow State University, Moscow 119991, Russia, E-mail: fedyanin@nanolab.phys.msu.ru. <https://orcid.org/0000-0003-4708-6895>

Dmitry N. Gulkin, Anna A. Popkova, Boris I. Afinogenov and Daniil A. Shilkin, Faculty of Physics, Lomonosov Moscow State University, Moscow 119991, Russia, E-mail: gulkin@nanolab.phys.msu.ru (D. N. Gulkin), popkova@nanolab.phys.msu.ru (A. A. Popkova), afinogenov@nanolab.phys.msu.ru (B. I. Afinogenov), shilkin@nanolab.phys.msu.ru (D. A. Shilkin). <https://orcid.org/0000-0002-7694-7204> (D. N. Gulkin). <https://orcid.org/0000-0001-7597-2734> (D. A. Shilkin)

Kęstutis Kuršelis and Boris N. Chichkov, Leibniz Universität Hannover, Institut für Quantenoptik, Hannover 30167, Germany, E-mail: kestutis.kurselis@lnqe.uni-hannover.de (K. Kuršelis), chichkov@iqo.uni-hannover.de (B. N. Chichkov). <https://orcid.org/0000-0002-8129-7373> (B. N. Chichkov)

Vladimir O. Bessonov, Faculty of Physics, Lomonosov Moscow State University, Moscow 119991, Russia; and Frumkin Institute of Physical Chemistry and Electrochemistry, Russian Academy of Sciences, Moscow 119071, Russia, E-mail: bessonov@nanolab.phys.msu.ru

waveguides [18, 19], lenses [20, 21], resonators [22, 23], and interferometers [13] have been realized. Less attention has been paid to the BSW excitation methods compatible with the concept of integrated photonics. Since the BSW wave vector is larger than the wave vector of light in air, special schemes are currently in use for the BSW excitation. The most common is a prism-based Kretschmann scheme [24, 25]. The scheme is bulky, requires oblique incidence and transparency of the substrate. In contrast, miniature diffraction gratings [26, 27] have much smaller footprint, but their fabrication becomes extremely complicated when unidirectional excitation is required [28].

Recently, high-index dielectric structures exhibiting pronounced optical Mie resonances have profoundly expanded the toolbox for optical engineering and have been shown to be useful in a variety of applications including Purcell enhancement of both electric [29] and magnetic [30] dipole emission, tunable directional scattering [31], and enhanced harmonic generation [32–35]. Variation of the particle geometry opens up an opportunity to control radiation patterns by tailoring the spectral position of different resonant modes [36, 37]. The interference of electric and magnetic dipoles leads to directional light scattering [38–40], that in turn can cause excitation of surface states and guided modes [41–43]. The concept of using optically resonant high-index nanoparticles for the excitation of surface electromagnetic waves was suggested in Ref. [41]. It has been shown that the light scattering by a silicon particle located on the surface of a metal film can lead to the directional excitation of surface plasmon–polaritons.

In this work, we demonstrate both experimentally and numerically the excitation of Bloch surface waves using subwavelength Mie-resonant silicon particles fabricated by the laser-induced backward transfer technique [44, 45] on the surface of a one-dimensional photonic crystal. Due to the excitation of various Mie-type resonances in the particle, color-selective directional coupling to the BSW mode is achieved. Numerical simulation supports the experiment and gives an estimate of 8% BSW excitation efficiency with a single nanoparticle for the proposed illumination scheme.

## 2 Results and discussion

The idea behind our experiment is that a Mie-resonant silicon nanoparticle (NP) atop a one-dimensional photonic crystal will mediate the excitation of the BSW. Accordingly, we illuminate the particle at a nonzero angle of incidence and use the back focal plane imaging technique [13, 31, 46, 47] to study properties of the excited BSW.

The studied system is schematically shown in Figure 1(a). Silicon nanoparticles are placed on the surface of a one-dimensional photonic crystal (PC). The PC parameters were optimized by the transfer matrix method [48] to sustain long-range TE-polarized BSWs in the spectral range from 650 to 900 nm. The resulting structure consists of 10 pairs of alternating layers of SiO<sub>2</sub> (refractive index  $n_{\text{SiO}_2}$  at 800 nm is equal to 1.45) and Ta<sub>2</sub>O<sub>5</sub> ( $n_{\text{Ta}_2\text{O}_5} = 2.07$ ) with thicknesses of 204 and 143 nm, respectively, deposited on a 170  $\mu\text{m}$ -thick glass substrate. Figure 1(b) shows the dispersions of the BSW and PC waveguide modes that occur in the studied spectral region. The spectral-angular dependence of the PC reflection coefficient demonstrating all excited modes of the structure is shown in Figure S1 (see Supplementary Materials). The effective refractive index of BSW ( $n_{\text{eff}}$ ), that is the ratio of the BSW propagation

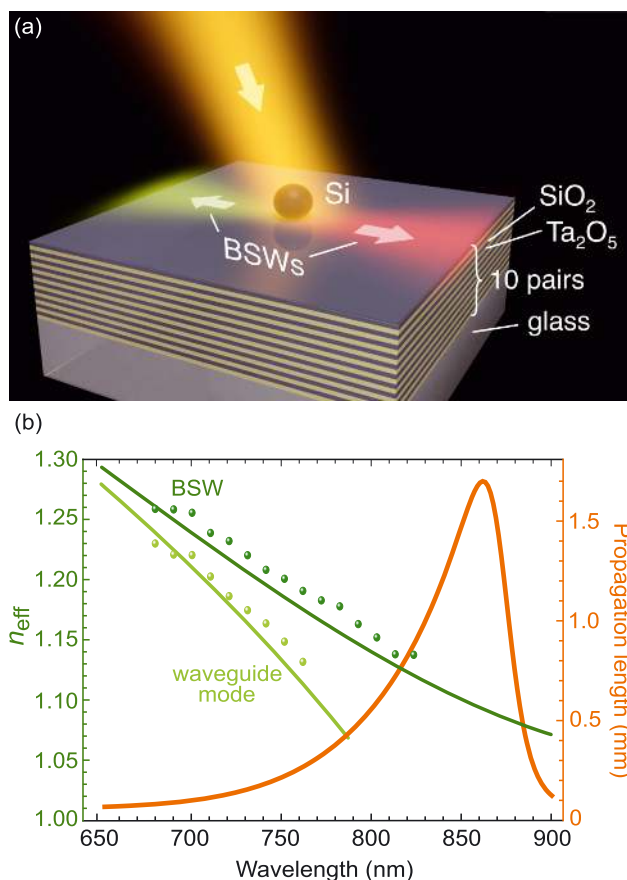


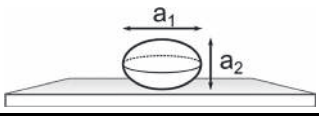
**Figure 1:** (a) Sketch of the idea: Color-selective excitation of Bloch surface waves (BSWs) as a result of directional light scattering at a Mie-resonant silicon nanoparticle. (b) Spectral dependences, measured (green dots) and calculated (green curves), of the effective refractive index  $n_{\text{eff}}$  for BSWs (dark green colors) and waveguide mode (light green colors), and BSW propagation length (orange curve).

constant  $k_{\text{BSW}}$  and the radiation wavevector in vacuum  $k_0$ , changes from 1.29 to 1.07 (Figure 1(b)). The orange curve depicts the dependence of BSW propagation length on the pump wavelength and demonstrates nonmonotonic behavior reaching the maximum value of approximately 1.5 mm near the 860 nm wavelength. As the wavelength decreases, the maximum of the BSW electromagnetic field shifts from the surface deep into the upper layer of the PC, which leads to an increase in radiation leakage and, as a result, a reduce in the propagation length. At wavelength longer than 860 nm, BSW is spectrally close to the edge of the photon band gap, which leads to a decrease in the quality factor of the resonance and also reduces the propagation length.

Silicon nanoparticles were deposited on the PC surface using the laser-induced backward transfer technique (see Methods for details). We fabricated a set of nanoparticles with sizes ranging from 150 to 210 nm that made it possible to excite Mie resonances in the visible and near-infrared (NIR) spectral range. The actual sizes of individual particles were measured by atomic force microscopy (AFM) and scanning electron microscopy (SEM). Table 1 shows the sizes used for further numerical calculations.

We study the BSW excitation with the leakage radiation microscopy technique, the scheme of which is shown in Figure 2 (see Methods for details). TE-polarized laser radiation illuminated the silicon particle through an objective lens with a numerical aperture (NA) of 0.95 focusing the laser beam into a  $1 \mu\text{m}$  spot at the sample surface. The desirable angle of incidence  $\theta = 25^\circ$  was achieved by

**Table 1:** Parameters of the studied nanoparticles (NP) used in the simulations:  $a_1$  is the equatorial diameter of the spheroid,  $a_2$  is the polar diameter.



Sample	$a_1$ (nm)	$a_2$ (nm)
NP1	152	136
NP2	168	158
NP3	190	176
NP4	212	184

parallel shift of the beam within the input aperture of the focusing objective lens and was controlled by determining the position of the pump spot at the back focal plane (BFP) image. The scattering of incident light by the nanoparticle leads to the excitation of the BSW that partially radiates (leaks) into the substrate. We detect BSW propagation by collecting leakage radiation using an oil-immersion objective lens with NA of 1.3. The intensity of leakage radiation is proportional to the BSW intensity. The direction of BSW propagation can be visualized by constructing the image of BFP of the collecting lens, in which the studied mode appears as a narrow bright ring with an asymmetrical intensity dependence on the azimuthal angle  $\varphi$  measured from the plane of incidence. The light intensity in the ring for a certain azimuthal angle  $\varphi$  (Figure 2(a)) corresponds to the amount of BSW energy propagating along the PC

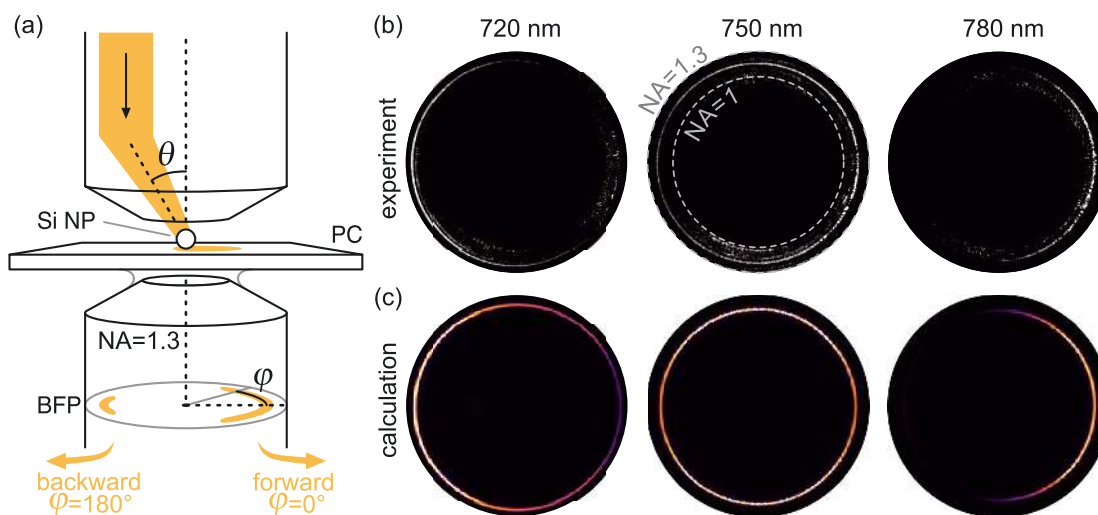


**Figure 2:** (a) Sketch of the leakage radiation microscopy scheme: Si NP is silicon nanoparticle; PC is photonic crystal; BFP is back focal plane; NA is numerical aperture. (b) Experimental images of the back focal plane for various excitation wavelengths (for NP4). The bright circle between  $\text{NA} = 1$  and  $\text{NA} = 1.3$  corresponds to the BSW. (c) Numerical simulation of the back focal plane images.

surface in that direction. Thus, by analyzing the dependence of the leakage radiation intensity on the azimuthal angle, it is possible to determine the directivity of the BSWs excited by the nanoparticle.

BFP images for the NP4 nanoparticle are shown in Figure 2(b) for three wavelengths demonstrating the cases of BSW excitation mainly backward, omnidirectional, and forward. The diameter of the leakage radiation ring is governed by the BSW effective refractive index and changes in accordance with the BSW dispersion law when tuning the wavelength. Since  $n_{\text{eff}}$  of the BSW is greater than unity, the ring is located outside the light cone denoted as the ring with  $\text{NA} = 1$ . By measuring the diameter of the rings, we can determine the dispersion law of the BSW and PC waveguide mode that appears as a barely visible ring with a slightly smaller diameter than that of the BSW ring. The resulting spectra of the effective refractive index of the modes are shown in Figure 1(b) by dots and are in good agreement with theoretical predictions. As the studied particles support Mie-type resonances in NIR spectral ranges, the direction of the light scattered by them depends on the wavelength of the incident light [37]. For the  $25^\circ$  angle of incidence, the 210 nm particle excites BSWs predominantly forward at the wavelength of 720 nm, while for the

wavelength of 780 nm the excitation occurs predominantly backwards (Figure 2(b)). A similar directional excitation is observed in numerical calculations (Figure 2(c)) performed by the finite-difference time-domain (FDTD) method using the Lumerical software package. The complete dynamical picture of the wavelength depended change in the direction of the BSW excitation is presented in the Supplementary Video.

Since Mie resonances shift to the red part of the spectrum with increasing particle size, the spectral position of the BSW switching region (changing the propagation direction from backward to forward) depends on the particle size as well. Figure 3 (top row) shows the efficiency of the BSW excitation as a function of the azimuthal angle  $\varphi$  and the wavelength of the incident light measured for studied particles. The images are obtained by processing the BFP images using the ring scan method (see Methods for details) and possess different azimuthal dependencies of the BSW excitation efficiency on the wavelength. For small NP1 and NP2 particles, BSW is excited predominantly forward in the entire studied spectral range. When the particle size increases, the switching region and more effective backward excitation are observed at short wavelengths. Starting from particle sizes of 200 nm (NP4 case),

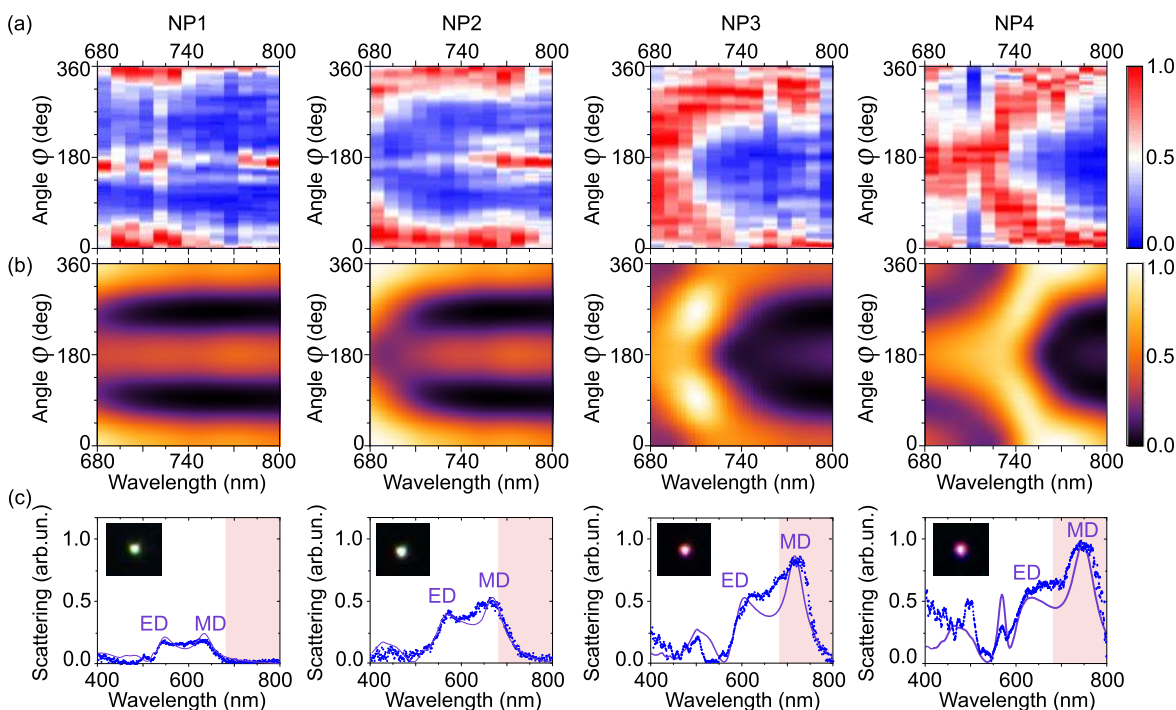


**Figure 3:** Measured (a) and calculated (b) efficiencies of the BSW excitation as a function of the pump wavelength and the azimuthal angle for various nanoparticle (NP) sizes. (c) Experimental (dots) and calculated (curves) scattering spectra of the particles: ED is electric dipole resonance; MD is magnetic dipole resonance. The insets show dark-field images of the particles; the shaded areas demonstrate the spectral range of the BFP measurements.



forward direction is suppressed at wavelengths from 680 to 730 nm, and backward BSW propagation is dominated. The complete switching from backward to forward direction of the BSW excitation is observed over a 30-nm wide spectral region; for wavelength longer than 760 nm the only forward BSW excitation is observed. Thereby, the nanoparticle can be used as subwavelength multiplexers within the 30-nm spectral range. Such behavior was proved by numerical simulations (see Methods for details). The calculated spectral-angular efficiency of the BSW excitation by particles of different sizes is shown in Figure 3(b). The experimental results are in good agreement with the results of numerical calculations and demonstrate that the regions of directional excitation are red-shifted with an increase in the particle size, as well as the Mie resonances.

The measured and calculated scattering spectra of the studied particles are represented in Figure 3(c). The spectra show that the BSW direction switching region corresponds to the position of the magnetic dipole (MD) resonance of the particle. The predominant forward excitation is observed on the long-wavelength slope of the MD resonance. In the region of electric dipole (ED) resonance, the backward wave excitation becomes predominant. The directivity of the BSW excitation can be estimated by introducing its numerical characteristic as the ratio of the energy of BSW propagating in a certain range of angles  $\varphi_0 \pm \Delta\varphi$  to the total energy of BSW propagating in all directions. Using data from Figure 3(b) (NP4 case), we obtained the spectral dependence of the directivity for the cases of BSW excitation forward ( $\varphi_0 = 0^\circ$ ) and backward ( $\varphi_0 = 180^\circ$ ) at  $\Delta\varphi = 22.5^\circ$ . The dependence is shown in Figure S2 and demonstrates that the maximum directivity reaches 60% for the forward BSW at a wavelength of approximately 760 nm and 50% for the backward BSW at a wavelength of approximately 720 nm, respectively.

The maximum value of BSW excitation efficiency obtained by integrating calculated spectral-angular efficiency of the BSW excitation over all azimuthal angles is observed for the NP4 particle and 750-nm wavelength and is approximately 8% (see Methods for details). The spectral dependence of the device efficiency has a non-monotonic behavior and decreases at a distance from 750 nm (see Figure S3 of Supplementary Materials). The efficiency of the nanocoupler also strongly depends on the beam size, since only part of the radiation interacts with the particle. As the beam size increases, a smaller part of the radiation falls into the scattering region of the particle and efficiency of BSW excitation decreases. We calculated the coupling efficiency for various Gaussian beam sizes

and NP4 particle. The obtained values are 8, 2 and 1% for 1  $\mu\text{m}$ , 5  $\mu\text{m}$ , and 10  $\mu\text{m}$  beam diameters, respectively. We have also calculated the efficiency of BSW excitation in the Kretschmann prism configuration for the same beam diameters and efficiencies are 0.5, 3 and 7%, respectively (see Figure S4). With the decrease in its size, the beam becomes more divergent and fewer angular components coincide with the BSW resonance, which decreases the excitation efficiency in the Kretschmann scheme. Thus, the proposed Mie-resonant nanocoupler turns out to be more effective for tightly focused beams in comparison with the Kretschmann scheme.

One of the main advantages of photonic crystals as an integrated photonic platform is the possibility of tuning the dispersion of the supported waveguide modes by varying the structure parameters. This idea can be applied to the studied system in order to shift the operating wavelengths to the visible range or to use higher-order Mie resonances for greater control over the direction of propagating modes. Figure 4 shows the properties of the BSW nanocouplers obtained numerically for the structures with varied geometrical parameters. Figure 4(a) shows the directional BSW excitation in the NIR spectral region for the PC parameters used in the experiment. To shift into the visible spectral range, the optical thicknesses of the PC layers must be reduced. Figure 4(b) shows the PC consisting of alternating layers of  $\text{SiO}_2$  and  $\text{Ta}_2\text{O}_5$  with thicknesses of 143 and 101 nm, respectively, sustaining BSW excitation in the spectral range from 450 to 700 nm. To achieve directional BSW excitation in the visible range, we must use a smaller particle since ED and MD resonances blueshift with the decrease in NP size. Thereby, an example of 110 nm silicon nanoparticle is presented in Figure 4(b) showing the ease of scaling the system. Another approach is to use larger nanoparticles that allow for a more complicated BSW excitation diagram due to quadrupole and high-order Mie resonances (Figure 4(c)). In addition, one can use a particle of another shape available for fabrication, such as a cube or a cylinder, which can give even more freedom in controlling the directivity of the excitation of waveguide modes [49].

The observed effects open up a variety of opportunities for advanced light manipulation in planar BSW-based photonic devices. Subwavelength nanoparticles can be used for color-selective coupling of light from free space to specific modes of integrated waveguides and resonators. In the case of particles hovering above a PC surface, the directional excitation of BSWs is accompanied by the appearance of optical forces [50] and can be used for in-plane sorting of particles according to their optical

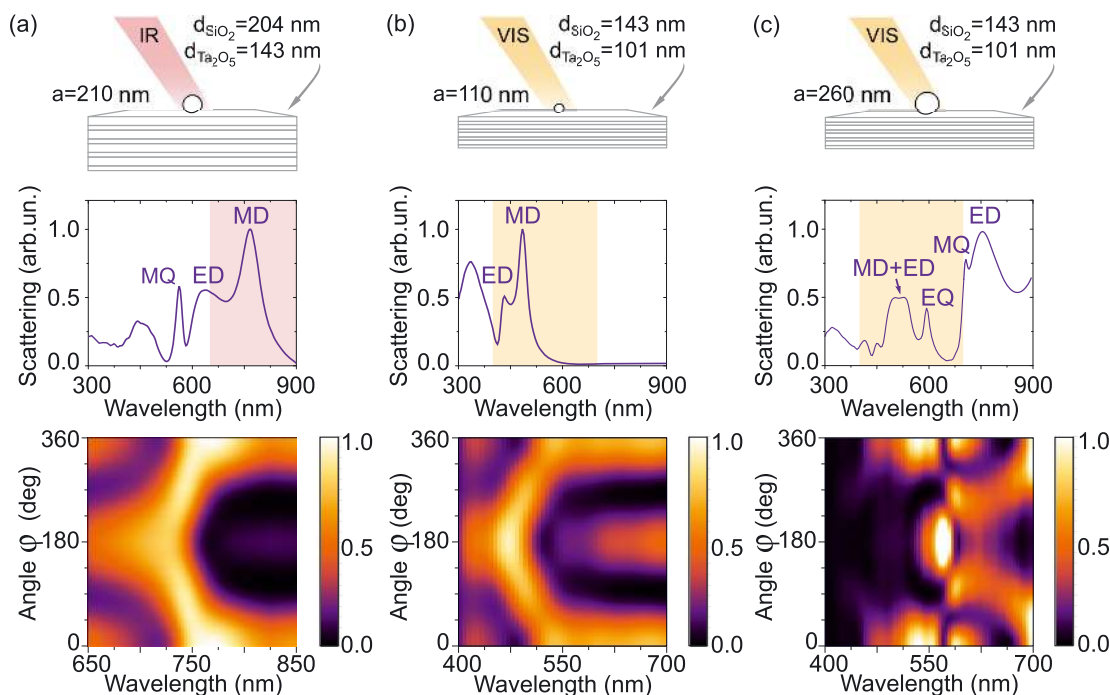


**Figure 4:** Schemes of 3 simulation cases (up row), their scattering cross-sections (middle row) and efficiency of Bloch surface wave (BSW) excitation (down row): IR is red and infrared spectral range; VIS is visible spectral range; ED is electric dipole resonance; MD is magnetic dipole resonance; EQ is electric quadrupole resonance; MQ is magnetic quadrupole resonance.

resonances [51]. Such a feature of the BSW platform as access to an optical field concentrated on the PC surface in combination with directional BSW excitation can be used to implement active integrated optical devices for sensing [52], strong light–matter coupling [53], or enhancing nonlinear optical effects [54].

### 3 Conclusions

We demonstrate the directional color-selective Bloch surface wave excitation by silicon Mie-resonant nanoparticles. Due to the versatile fabrication technique by laser-induced transfer, nanoparticles can be easily integrated into various platforms, for example, deposited at the surface of a one-dimensional PC. By tuning the parameters of the particles for the effective excitation of certain Mie resonances, it is possible to accomplish directional excitation of BSWs in both forward and backward directions. The ability to vary the system parameters, such as PC layer thicknesses and materials and particle size, enables achieving more complicated diagrams of BSW excitation. Adjusting the dispersion of the supported modes by changing the PC geometry allows one to shift the working spectral range to the visible part of the spectrum.

## 4 Methods

### 4.1 Fabrication of nanoparticles

The particles have been fabricated using the laser-induced backward transfer (LIBT) technique, also referred to as femtosecond laser printing [45, 55]. This technique is based on focusing a single laser pulse on a target film, which causes its melting and formation of a particle with a momentum directed from the target substrate. The technique allows one to produce isolated close-to-spherical particles with a controllable size and place them on a broad range of substrates in a controllable manner.

We used a commercial laser system (Tsunami femtosecond oscillator and Spitfire regenerative amplifier, Spectra Physics) providing laser pulses with a central wavelength of 800 nm and a nominal pulse duration of 40 fs; the repetition rate was set to 10 Hz. To control the optical power, the laser output was passed through a half-wave plate, a Glan prism, and a stack of absorptive neutral density optical filters. The pulse energy in the passed beam during the particle fabrication process was estimated as 17 nJ. The beam was focused on the target substrate using a 50 $\times$  Nikon microscope objective lens with an NA of 0.45; this corresponds to the waist diameter of 1.1  $\mu\text{m}$ . As a target, we used a silicon-on-insulator (SOI) wafer with a 50 nm upper single-crystalline silicon layer and a 200 nm silicon dioxide layer. In the transfer region, the distance between the target and the PC was at least 20  $\mu\text{m}$ , which provided the creation of crystalline particles [56]. During the transfer process, the sample was moved on a translation stage with a constant velocity, while the target was irradiated by

single laser pulses. The distance between the neighboring shots was set to 25  $\mu\text{m}$ , allowing us to work with individual particles in further experiments.

## 4.2 Leakage radiation microscopy

We used a home-build leakage radiation microscopy setup allowing the BFP visualization [13, 47]. Ti:Sapphire laser (Coherent Chameleon) was used to obtain a linearly polarized radiation tuning in the spectral range from 680 to 1000 nm. The radiation was focused on the PC surface into a 1  $\mu\text{m}$  spot using an objective lens with  $\text{NA} = 0.95$ . In this case, the focusing NA was approximately 0.45. Hence, the central angle of incidence was chosen equal to  $25^\circ$  to avoid clipping the beam at the entrance pupil of the objective lens. The leakage radiation transmitted through the PC and the substrate was collected using an oil-immersion objective lens (100 $\times$ ,  $\text{NA} = 1.3$ , Olympus). For further spatial filtering, intermediate images of the direct and back focal planes were constructed. In the direct intermediate image, we placed a round block over the particle image to cut off an image area with a radius of about 10  $\mu\text{m}$  around the particle, blocking its scattering and the transmitted laser beam. As the result, only leakage radiation of BSW propagating outside the blocked area was detected, along with weak scattered radiation. To highlight the area of interest and improve the visibility of particles, an additional round block in the intermediate BFP image was used, eliminating the area with a radius corresponding to  $\text{NA} \leq 1$ .

## 4.3 BFP image processing

The dependence of the BSW leakage radiation intensity on the azimuthal angle, shown in Figure 3(a), was obtained by processing the BFP images recorded by a 16-bit CMOS camera (Thorlabs CS2100M). Each point of the BFP image can be represented in a polar coordinate system with certain values of the wavevector of light  $n_{\text{eff}}$  and its propagation angle  $\varphi$  relative to the incidence plane of the laser beam. Since BSW has the same wavevector value regardless of the propagation direction, it appears as a narrow ring in the BFP image (see Figure 2). For each wavelength, we determined the diameter and center of the BSW ring. Then, the ring was divided into the sectors with a step of  $\Delta\varphi = 1^\circ$ . For each  $\varphi$ , the BSW intensity was found as the sum of intensity values in all pixels located within the ranges both for the angle  $[\varphi; \varphi + \Delta\varphi]$  and the wavevector  $[n_{\text{eff}} - \Delta n; n_{\text{eff}} + \Delta n]$ , where  $\Delta n$  is determined by the width of the BSW ring and is about 0.03. The dependence of the BSW intensity on the azimuthal angle obtained in this way was smoothed out, normalized to its maximum, and plotted as a column on the graph in Figure 3(a).

## 4.4 Numerical simulations

The numerical simulation of directional BSW excitation was performed using the commercial Lumerical FDTD Solutions software package. The model sample was a one-dimensional PC of experimental parameters on a semi infinite fused silica substrate. A silicon nanoparticle was located on the PC surface. Ellipsoidal particles were selected with sizes according to Table 1 to simulate the experiment. For the systems shown in Figure 4(b) and (c), spherical particles were used. The calculations were performed for both crystalline

and amorphous silicon. The best agreement with experiment was found for the crystalline particles as expected for the case of LIBT with a 20  $\mu\text{m}$  distance between the donor and receiving substrates.

To calculate the directivity of the BSW excitation, an array of one-dimensional monitors oriented across the PC surface was located at a distance of 3  $\mu\text{m}$  around the particle in a circle with a step of  $1^\circ$ . Each monitor measured the distribution of the electromagnetic field inside the PC layers and in the area of BSW attenuation in air. The radiation transmitted through the monitor is a combination of incident and scattered radiation. To determine how much of this radiation transfers to BSW, the overlap integral between the field distribution measured by the monitor and the BSW field distribution was calculated. The BSW field distribution depending on the wavelength was calculated using mode source function and is shown in Figure S5 of Supplementary Materials.

The efficiency of BSW excitation was obtained as a product of the overlap integral and the ratio of the flux of the Poynting vector through the PC cross-section to the incident one.

The result value of the device efficiency was found by integrating the calculated values of BSW excitation efficiency for all azimuthal angles. The maximum efficiency is observed for NP4 nanoparticles and is 8% obtained for the 750 nm wavelength and 1  $\mu\text{m}$  beam diameter.

The BFP images (Figure 1(c)) were simulated using the Fourier transform (far-field transformation) from the near-field distribution in the upper layer of PC. By analogy with the experiment, the region with  $\text{NA} \leq 1$  was excluded from consideration.

**Acknowledgement:** The authors acknowledge technical assistance from Natalia G. Kokareva. We thank Denis M. Zhigunov and Kirill R. Safronov for fruitful discussions.

**Author contribution:** All the authors have accepted responsibility for the entire content of this submitted manuscript and approved submission.

**Research funding:** The work was performed under financial support of the Russian Ministry of Education and Science (Grant No. 14.W03.31.0008) and MSU Quantum Technology Centre and according to the Development program of the Interdisciplinary Scientific and Educational MSU School “Photonic and Quantum technologies. Digital medicine”. B.I.A. thanks the Russian Science Foundation (Grant No. 19-72-00170). B.N.C. acknowledges financial support from the Deutsche Forschungsgemeinschaft (DFG, German Research Foundation) under Germany’s Excellence Strategy within the Cluster of Excellence PhoenixD (EXC 2122, Project ID 390833453) and the Cluster of Excellence QuantumFrontiers (EXC 2123, Project ID 390837967). A.A.F. thanks the Russian Science Foundation (Grant No. 20-12-00371) and the Russian Foundation for Basic Research (Grant No. 18-29-20097).

**Conflict of interest statement:** The authors declare no conflicts of interest regarding this article.

## References

- [1] J. Wang, S. Paesani, Y. Ding, et al., “Multidimensional quantum entanglement with large-scale integrated optics,” *Science*, vol. 360, no. 6386, pp. 285–291, 2018.
- [2] D. Erickson, X. Xavier, Y.-F. Chen, and S. Mandal, “Nanomanipulation using near field photonics,” *Lab Chip*, vol. 11, no. 6, pp. 995–1009, 2011.
- [3] M.-C. Estevez, M. Alvarez, and L. M. Lechuga, “Integrated optical devices for lab-on-a-chip biosensing applications,” *Laser Photon. Rev.*, vol. 6, no. 4, pp. 463–487, 2012.
- [4] D. Akinwande, C. Huyghebaert, C.-H. Wang, et al., “Graphene and two-dimensional materials for silicon technology,” *Nature*, vol. 573, no. 7775, pp. 507–518, 2019.
- [5] V. J. Sorger, R. F. Oulton, R.-M. Ma, and X. Zhang, “Toward integrated plasmonic circuits,” *MRS Bull.*, vol. 37, no. 8, pp. 728–738, 2012.
- [6] B. I. Afinogenov, V. O. Bessonov, A. A. Nikulin, and A. A. Fedyanin, “Observation of hybrid state of Tamm and surface plasmon-polaritons in one-dimensional photonic crystals,” *Appl. Phys. Lett.*, vol. 103, no. 6, 2013, Art no. 061112.
- [7] B. I. Afinogenov, V. O. Bessonov, and A. A. Fedyanin, “Second-harmonic generation enhancement in the presence of Tamm plasmon–polaritons,” *Opt. Lett.*, vol. 39, no. 24, pp. 6895–6898, 2014.
- [8] D. A. Shilkin, E. V. Lyubin, I. V. Soboleva, and A. A. Fedyanin, “Direct measurements of forces induced by Bloch surface waves in a one-dimensional photonic crystal,” *Opt. Lett.*, vol. 343, pp. 4883–4886, 2015.
- [9] B. I. Afinogenov, V. O. Bessonov, I. V. Soboleva, and A. A. Fedyanin, “Ultrafast all-optical light control with Tamm plasmons in photonic nanostructures,” *ACS Photonics*, vol. 6, pp. 844–850, 2019.
- [10] P. Yeh, A. Yariv, and A. Y. Cho, “Optical surface waves in periodic layered media,” *Appl. Phys. Lett.*, vol. 32, pp. 104–105, 1978.
- [11] W. Robertson and M. May, “Surface electromagnetic wave excitation on one-dimensional photonic band-gap arrays,” *Appl. Phys. Lett.*, vol. 74, pp. 1800–1802, 1999.
- [12] T. Kovalevich, D. Belharet, L. Robert, et al., “Bloch surface waves at the telecommunication wavelength with lithium niobate as the top layer for integrated optics,” *Appl. Opt.*, vol. 58, pp. 1757–1762, 2019.
- [13] K. R. Safronov, D. N. Gulkin, I. M. Antropov, K. A. Abrashitova, V. O. Bessonov, and A. A. Fedyanin, “Multimode interference of Bloch surface electromagnetic waves,” *ACS Nano*, vol. 14, pp. 10428–10437, 2020.
- [14] R. Dubey, E. Barakat, M. Häyrynen, et al., “Experimental investigation of the propagation properties of Bloch surface waves on dielectric multilayer platform,” *J. Eur. Opt. Soc. Rapid*, vol. 13, pp. 1–9, 2017.
- [15] T. Perani and M. Liscidini, “Long-range Bloch surface waves in photonic crystal ridges,” *Opt. Lett.*, vol. 45, pp. 6534–6537, 2020.
- [16] I. V. Soboleva, V. V. Moskalenko, and A. A. Fedyanin, “Giant Goos–Hänchen effect and Fano resonance at photonic crystal surfaces,” *Phys. Rev. Lett.*, vol. 108, p. 123901, 2012.
- [17] R. Badugu, J. Mao, S. Blair, et al., “Bloch surface wave-coupled emission at ultraviolet wavelengths,” *J. Phys. Chem. C*, vol. 120, pp. 28727–28734, 2016.
- [18] E. Descrovi, T. Sfez, M. Quaglio, et al., “Guided Bloch surface waves on ultrathin polymeric ridges,” *Nano Lett.*, vol. 343, pp. 2087–2091, 2010.
- [19] T. Sfez, E. Descrovi, L. Yu, et al., “Bloch surface waves in ultrathin waveguides: near-field investigation of mode polarization and propagation,” *J. Opt. Soc. Am. B*, vol. 27, pp. 1617–1625, 2010.
- [20] L. Yu, E. Barakat, T. Sfez, L. Hvozdar, J. Di Francesco, and H. P. Herzig, “Manipulating Bloch surface waves in 2D: a platform concept-based flat lens,” *Light Sci. Appl.*, vol. 3, pp. e124, 2014.
- [21] Y. Augenstein, A. Vetter, B. V. Lahijani, H. P. Herzig, C. Rockstuhl, and M.-S. Kim, “Inverse photonic design of functional elements that focus Bloch surface waves,” *Light Sci. Appl.*, vol. 7, pp. 1–9, 2018.
- [22] R. Dubey, B. V. Lahijani, E. Barakat, et al., “Near-field characterization of a Bloch-surface-wave-based 2D disk resonator,” *Opt. Lett.*, vol. 41, pp. 4867–4870, 2016.
- [23] G. Rodriguez, D. Aurelio, M. Liscidini, and S. Weiss, “Bloch surface wave ring resonator based on porous silicon,” *Appl. Phys. Lett.*, vol. 115, 2019, Art no. 011101.
- [24] E. Kretschmann, “Decay of non radiative surface plasmons into light on rough silver films. Comparison of experimental and theoretical results,” *Opt. Commun.*, vol. 6, pp. 185–187, 1972.
- [25] V. Koju and W. M. Robertson, “Excitation of Bloch-like surface waves in quasi-crystals and aperiodic dielectric multilayers,” *Opt. Lett.*, vol. 41, pp. 2915–2918, 2016.
- [26] T. Kovalevich, P. Boyer, M. Suarez, et al., “Polarization controlled directional propagation of Bloch surface wave,” *Opt. Express*, vol. 25, pp. 5710–5715, 2017.
- [27] R. Wang, Y. Wang, D. Zhang, et al., “Diffraction-free Bloch surface waves,” *ACS Nano*, vol. 11, pp. 5383–5390, 2017.
- [28] R. Marchetti, C. Lacava, A. Khokhar, et al., “High-efficiency grating-couplers: demonstration of a new design strategy,” *Sci. Rep.*, vol. 7, pp. 1–8, 2017.
- [29] V. Rutckaia, F. Heyroth, A. Novikov, M. Shaleev, M. Petrov, and J. Schilling, “Quantum dot emission driven by Mie resonances in silicon nanostructures,” *Nano Lett.*, vol. 17, pp. 6886–6892, 2017.
- [30] A. Vaskin, S. Mashhadi, M. Steinert, et al., “Manipulation of magnetic dipole emission from  $\text{Eu}^{3+}$  with Mie-resonant dielectric metasurfaces,” *Nano Lett.*, vol. 19, pp. 1015–1022, 2019.
- [31] T. Shibanuma, T. Matsui, T. Roschuk, et al., “Experimental demonstration of tunable directional scattering of visible light from all-dielectric asymmetric dimers,” *ACS Photonics*, vol. 4, pp. 489–494, 2017.
- [32] S. Kruk and Y. Kivshar, “Functional meta-optics and nanophotonics governed by Mie resonances,” *ACS Photonics*, vol. 4, pp. 2638–2649, 2017.
- [33] M. K. Kroychuk, D. F. Yagudin, A. S. Shorokhov, et al., “Tailored nonlinear anisotropy in Mie-resonant dielectric oligomers,” *Adv. Opt. Mater.*, vol. 7, p. 1900447, 2019.



- [34] M. K. Kroychuk, A. S. Shorokhov, D. F. Yagudin, et al., “Enhanced nonlinear light generation in oligomers of silicon nanoparticles under vector beam illumination,” *Nano Lett.*, vol. 20, pp. 3471–3477, 2020.
- [35] L. Carletti, A. Locatelli, O. Stepanenko, G. Leo, and C. De Angelis, “Enhanced second-harmonic generation from magnetic resonance in AlGaAs nanoantennas,” *Opt. Express*, vol. 23, pp. 26544–26550, 2015.
- [36] I. Staude, A. E. Miroschnichenko, M. Decker, et al., “Tailoring directional scattering through magnetic and electric resonances in subwavelength silicon nanodisks,” *ACS Nano*, vol. 7, pp. 7824–7832, 2013.
- [37] Y. H. Fu, A. I. Kuznetsov, A. E. Miroschnichenko, Y. F. Yu, and B. Luk’yanchuk, “Directional visible light scattering by silicon nanoparticles,” *Nat. Commun.*, vol. 4, p. 1527, 2013.
- [38] G. Videen and W. S. Bickel, “Light-scattering resonances in small spheres,” *Phys. Rev. A*, vol. 45, p. 6008, 1992.
- [39] J.-M. Geffrin, B. García-Cámara, R. Gómez-Medina, et al., “Magnetic and electric coherence in forward-and back-scattered electromagnetic waves by a single dielectric subwavelength sphere,” *Nat. Commun.*, vol. 3, p. 1171, 2012.
- [40] S. Person, M. Jain, Z. Lapin, J. J. Sáenz, G. Wicks, and L. Novotny, “Demonstration of zero optical backscattering from single nanoparticles,” *Nano Lett.*, vol. 13, pp. 1806–1809, 2013.
- [41] I. S. Sinev, A. A. Bogdanov, F. E. Komissarenko, et al., “Chirality driven by magnetic dipole response for demultiplexing of surface waves,” *Laser Photon. Rev.*, vol. 11, p. 1700168, 2017.
- [42] J. E. Vázquez-Lozano, A. Martínez, and F. J. Rodríguez-Fortuño, “Near-field directionality beyond the dipole approximation: electric quadrupole and higher-order multipole angular spectra,” *Phys. Rev. Appl.*, vol. 12, 2019, Art no. 024065.
- [43] F. J. Rodríguez-Fortuño, G. Marino, P. Ginzburg, et al., “Near-field interference for the unidirectional excitation of electromagnetic guided modes,” *Science*, vol. 340, pp. 328–330, 2013.
- [44] A. I. Kuznetsov, J. Koch, and B. N. Chichkov, “Laser-induced backward transfer of gold nanodroplets,” *Opt. Express*, vol. 17, pp. 18820–18825, 2009.
- [45] U. Zywietz, A. B. Evlyukhin, C. Reinhardt, and B. N. Chichkov, “Laser printing of silicon nanoparticles with resonant optical electric and magnetic responses,” *Nat. Commun.*, vol. 5, p. 3402, 2014.
- [46] J. Li, N. Verellen, D. Vercruyssen, T. Bearda, L. Lagae, and P. Van Dorpe, “All-dielectric antenna wavelength router with bidirectional scattering of visible light,” *Nano Lett.*, vol. 16, pp. 4396–4403, 2016.
- [47] K. A. Abrashitova, D. N. Gulkin, K. R. Safronov, et al., “Bloch surface wave photonic device fabricated by femtosecond laser polymerisation technique,” *Appl. Sci.*, vol. 8, p. 63, 2018.
- [48] P. Yeh, A. Yariv, and C.-S. Hong, “Electromagnetic propagation in periodic stratified media: I. General theory,” *J. Opt. Soc. Am.*, vol. 67, pp. 423–438, 1977.
- [49] P. D. Terekhov, K. V. Baryshnikova, Y. A. Artemyev, A. Karabchevsky, A. S. Shalin, and A. B. Evlyukhin, “Multipolar response of nonspherical silicon nanoparticles in the visible and near-infrared spectral ranges,” *Phys. Rev. B*, vol. 96, no. 3, 2017, Art no. 035443.
- [50] N. Kostina, V. Bobrov, M. Petrov, and A. S. Shalin, “Optical pulling and pushing forces via Bloch surface waves,” arXiv preprint, 2021. <https://arxiv.org/abs/2104.01950>.
- [51] D. A. Shilkin, E. V. Lyubin, M. R. Shcherbakov, M. Lapine, and A. A. Fedyanin, “Directional optical sorting of silicon nanoparticles,” *ACS Photonics*, vol. 4, pp. 2312–2319, 2017.
- [52] A. Sinibaldi, N. Danz, E. Descrovi, et al., “Direct comparison of the performance of Bloch surface wave and surface plasmon polariton sensors,” *Sens. Actuators, B*, vol. 174, pp. 292–298, 2012.
- [53] F. Barachati, A. Fieramosca, S. Hafezian, et al., “Interacting polariton fluids in a monolayer of tungsten disulfide,” *Nat. Nanotechnol.*, vol. 13, pp. 906–909, 2018.
- [54] V. N. Konopsky, E. V. Alieva, S. Y. Alyatkin, A. A. Melnikov, S. V. Chekalin, and V. M. Agranovich, “Phase-matched third-harmonic generation via doubly resonant optical surface modes in 1D photonic crystals,” *Light Sci. Appl.*, vol. 5, p. e16168, 2016.
- [55] D. M. Zhigunov, A. B. Evlyukhin, A. S. Shalin, U. Zywietz, and B. N. Chichkov, “Femtosecond laser printing of single Ge and SiGe nanoparticles with electric and magnetic optical resonances,” *ACS Photonics*, vol. 5, pp. 3977–3983, 2018.
- [56] S. Makarov, L. Kolotova, S. Starikov, U. Zywietz, and B. Chichkov, “Resonant silicon nanoparticles with controllable crystalline states and nonlinear optical responses,” *Nanoscale*, vol. 10, pp. 11403–11409, 2018.

---

**Supplementary Material: Video 1.** Visualization of the color-sensitive directional BSW excitation.

**Supporting Document.** Spectra-angular dependence of PC reflection coefficient, maps of BSW field distribution inside photonic crystal, spectral dependence of the device efficiency, comparison diagram of the BSW excitation efficiency by a Si NP and the Kretschmann scheme for different beam diameters and spectral dependence of the BSW excitation directivity for NP4 nanoparticle.

The online version of this article offers supplementary material (<https://doi.org/10.1515/nanoph-2021-0295>).